applied sciences

MDPI

Article

New Simple Analytical Surge/Swab Pressure Model for Power-Law and Modified Yield-Power-Law Fluid in Concentric/Eccentric Geometry

Amir Mohammad * and Mesfin Belayneh

Department of Electrical Engineering & Computer Science, University of Stavanger, 4021 Stavanger, Norway; mesfin.a.belayneh@uis.no

* Correspondence: amir.mohammed@uis.no; Tel.: +47-951-29-664

Abstract: The axial movement of pipe in and out of the well generates positive (surge) and negative (swab) pressures that will impact the well pressure. When the swab and surge effects cause well pressures outside the allowable operational limits, wellbore instability (well collapse/well fracture), kick, and induced drill string sticking issues will occur. The problems increase the operational and nonproductive time-related costs. Consequently, the drilling budget rises significantly. It is therefore, imperative to predict the differential pressures in order to mitigate the problems. Even though several models have been developed in the past, models work for the considered experimental setup and conditions. In this paper, a simple analytical model was derived for eccentric/concentric annuli. The fluid rheological behaviors were assumed to be described by power law and yielded power-law. The model is derived based on a steady state condition, and the effects of tripping speed, the power-law fluids, the yield-power-law fluids rheological parameters, and well geometries are considered. The model is compared with experimental data from the literature and with the existing model. Parametric sensitivity studies have been conducted. Results show that the model prediction exhibited quite good performance, with an average percentile error deviation of 9.9% and 6.2% for the power-law and yield-power-law fluids, respectively. However, more testing is required to determine the model's limitations and application.

Keywords: swab; surge; simulation; machine learning modeling; oil-based drilling fluids

Citation: Mohammad, A.; Belayneh, M. New Simple Analytical Surge/Swab Pressure Model for Power-Law and Modified Yield-Power-Law Fluid in Concentric/Eccentric Geometry. *Appl. Sci.* **2023**, *13*, 12867. https://doi.org/10.3390/app132312867

Academic Editor: Jianzhong Lin

Received: 24 October 2023
Revised: 24 November 2023
Accepted: 25 November 2023
Published: 30 November 2023

1. Introduction

Accurate well pressure prediction is vital, especially in deep-water and horizontal drilling, where the narrow stability window poses challenges. Factors like fluid properties, geometry, eccentricity, flow rate, and tripping speeds play a crucial role. Incorrect predictions can lead to operational issues, higher costs, and wellbore instability.

The petroleum industry has made significant technological advancements, increasing drilling depth efficiency. However, nonproductive time (NPT) remains a concern, accounting for 25–30% of drilling operations according to Hovda et al. (2008) [1]. In deep-water environments like the Gulf of Mexico, downtime in gas wells from 1993–2003 amounted to approximately 40% of total time (Reham et al., 2013) [2]. NPT incidents like lost circulation, kicks, and stuck pipes are significant contributors (Pilisi et al., 2010) [3]. Wellbore-instability-related NPT alone increases drilling cost by 10% to 20% (Radden, 2009) [4].

Utilizing high-speed drill string telemetry can further improve the performance of drilling operations. High-speed telemetry allows for the reduction of nonproductive time (NPT) [1]. High-quality real-time data transfer and logging during drilling help drilling personnel make accurate, timely decisions (Thomas et al., 2018) [5]. For example, monitoring swabbing speed in the reservoir section can help prevent well pressure from dropping below formation and collapse pressures, averting fluid influx and well collapse.

Similarly, higher surging speed can lead to excessive pressure, causing circulation loss, which can be detected and addressed promptly using real-time data.

Accurate determination of tripping speed is essential for effective well-pressure management and cost reduction. Numerous swab and surge hydraulic models have been developed in the literature, considering factors like tripping speeds, fluid rheology, pipe/cement elasticity, viscous forces, well eccentricity, and string rotational speed. Based on experimental and field observations, these models address surge and swab effects under various conditions, including steady-state and dynamic/transient scenarios.

Effective pressure management is essential in drilling and well construction operations, especially with improved methods and technologies to perform drilling operations in extended-reach wells, slim holes, and casing while drilling. These advancements can lead to excessive surge pressure during tripping and drilling operations in the extended reach wells where the narrow operations windows persist. Failure to detect these down-hole pressure fluctuations can result in various drilling issues, including formation fracturing, lost circulation, kicks, and blowouts. These problems directly translate to higher budgets due to nonproductive downtime, equipment damage, and costly corrective measures. Consequently, developing an accurate surge pressure model becomes essential for precisely predicting tripping and casing running speed limits. Numerous studies have been undertaken to determine surge and swab pressures to optimize tripping operations. The following highlights some of the selected studies.

Burkhardt (1961) [6] developed a technique to estimate surge and swab pressures in Bingham plastic fluids, specifically emphasizing steady-state conditions. In 1964, Schuh utilized a comparable approach to formulate a power-law fluid model, assuming steady-state flow within a concentric annulus [7]. Fontenot and Clark (1974) devised a method of anticipating swab pressure in Bingham plastic and power-law fluids [8]. Mitchell (1988) presented a dynamic model with several novel elements, such as viscous forces, temperature changes, formation properties, pipe and cement elasticity, and mud rheology [9]. Ahmed et al. (2008) performed experiments to investigate the effect of pipe rotation on well pressure in concentric and eccentric annuli filled with xanthan gum and polyanionic cellulose-based fluids [10]. Crespo et al. (2010) crafted a streamlined surge and swab model for yield-power-law fluids [11]. Srivastav et al. (2017) laid out a model. They conducted an experimental study to demonstrate the impact of pipe velocity, mud properties, annular clearance, and pipe eccentricity on the surge and swab pressures [12]. Gjerstad et al. (2013) utilized a Kalman filter alongside differential pressure equations to predict and calibrate real-time surge and swab pressures for Herschel–Bulkley fluids [13]. Ming et al. created a prediction model for swabs and surges in concentric annuli using computational fluid dynamics methods in 2016. They attained an accuracy of up to 75% by comparing the results of experiments and simulations [14].

By considering fluid compressibility, formation, and pipe elasticity, Fredy et al. (2012) created a steady-state swab and surge prediction model using narrow slot geometry and regression techniques [15]. Erge et al. (2015) crafted a numerical model for estimating annular pressure loss in eccentric annuli [16]. He et al. (2016) utilized numerical simulations and regression techniques to forecast swab and surge pressures during drilling operations, achieving a maximum error of $\pm 3\%$ compared to experimental measurements [17]. Evren M. et al. (2018) investigated pressure loss using artificial neural network techniques and parametric studies [18]. An analytical model was built by Ettehadi et al. (2018) to compute pressure surges in Herschel–Bulkley fluids resulting from drill string movement [19]. Shwetank et al. (2020) created a two-layer neural network to forecast swab and surge pressures. They then conducted a parametric study to determine how different parameters affected swabs and surge pressures [20]. In 2021, Zakarya and co-authors employed numerical and random forest models to explore the dynamics of drilling fluid flow through an eccentric annulus during tripping operations.

Additionally, they examined the impact of eccentricity on annular velocity and perceived viscosity profiles [21]. Deep learning techniques were used by Amir et al. (2022) to

predict equivalent circulating mud density during tripping and drilling operations [22]. Amir et al. (2023) [23] also simulated the swab/surge phenomenon based on Bingham plastic, power-law, and Robertson and Stiff models. Results showed the inconsistency and the model prediction deviations among the models. Moreover, the work presented six machine learning models and predictions of the field telemetry swab dataset. Table 1 provides the reviewed swab / surge models for yield power law fluid behaviors along with the model controlling parameters.

Table 1. Summary of literature reviewed swab and surge models.

Authors	Research Focus and Parameters/Models	Fluid Rheology	Key Findings and Remarks
Crespo et al. (2010) [11]	Pressure Variations Resulting from String Pipe Reciprocation, Flow Slot Analysis, Conservation Equations, Input Fluid Properties, Borehole Geometry, and Pipe Velocity	Yield Power Law	Concentration on the effects of reciprocating pipe in steady-state flow.
Srivastav et al. (2017) [12]	Investigation of Eccentric and Concentric Annuli, Closed-End Pipes, and the Impact of Pipe Diameter Ratios and Fluid Rheological Properties	Herschel–Bulkley	Herschel–Bulkley analysis of steady-state flow with an emphasis on pipe geometry and rheology.
Oner Erge et al. (2015) [16]	Concentric and Eccentric Annuli, Reciprocating Pipe, Temperature Effect, Fluid Properties, and Borehole Geometry	Yield Power Law	Study of steady-state drilling conditions with various parameters.
He et al. (2016) [17]	Concentric Annulus, Diameter Ratios, Fluid Behavior	Yield Power Law	Analysis of steady-state drilling conditions.
Evren M. et al. (2018) [18]	Drill String Rotations, Eccentricity, Buckling Configurations	Yield Power Law	Application of neural network techniques.
Shwetank et al. (2020) [24]	Concentric Annulus, Diameter Ratio, Fluid Behavior Index, and Varying Tripping Speed	Yield Power Law	Comparative analysis of drilling parameters.

Motivation/Objective of This Paper

The reviewed scientific works indicate that swab and surge experimental have been performed based on the rheological models (i.e., power law, yield power law, Bingham plastic) in concentric and eccentric well-annular configurations. The pressure loss in an eccentric annulus is commonly computed based on the pressure loss in the concentric annulus and using the correlation factor. Among others, Haciislamoglu and Langlinais (1990) [25] developed empirical R-factors based on power-law fluids. It is important to note that in general, the reviewed literature often does not encompass all operational, fluid property, and wellbore geometry variations. Consequently, the applicability of the swab and surge models is valid within the scope of the assumed conditions and experimental setups.

For instance, Srivastav et al. (2017) [12] conducted experimental work demonstrating how trip speed, drilling fluid properties, annular clearance, and pipe eccentricity influence surge and swab pressures. The authors have also developed a model based on a narrow-slot approach to predict their experimental measured dataset. The model predicted the experimental data with certain discrepancies. Due to the availability of Srivastav et al.'s (2017) [12] experimental and model prediction dataset; this paper aims to develop a new pressure loss model based on a different approach and compare the model performances.

2. Modeling

A simplified analytical model was developed to calculate the pressure loss gradient for the power-law and yield-power-law fluid rheological models. This model applies to fluid flow within concentric and eccentric annular geometries under steady-state conditions. The analysis assumes laminar flow, and fluid is characterized by incompressibility. Additionally,

it considers a scenario without fluid circulation, in which the pipe moves vertically within the wellbore. A no-slip boundary condition is assumed at the interface between the pipe's outer diameter wall and the wellbore's inner wall. Figure 1 provides a visual representation of the drill string's motion within the wellbore, which induces the movement of the annular fluid. As shown in the figure, V_p is the speed of the string, r_p is the outer radius of the pipe, and R_h is the inner radius of the wellbore.

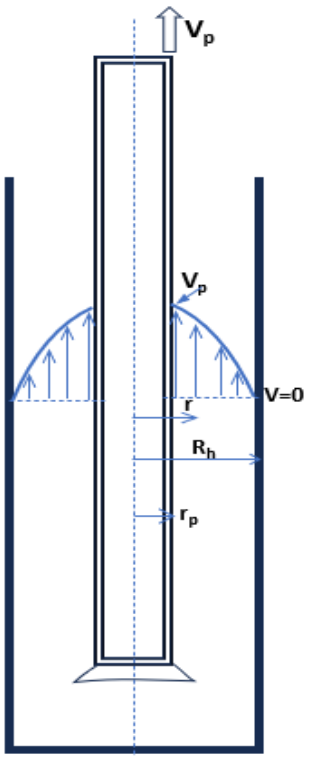

Figure 1. Tripping out while rig pump shut off.

Due to pressure difference, fluid flows from high pressure to low pressure. The fluid flow due to the external force is resisted by the shear force in the fluids. By employing the force balance analysis, the differential pressure over length can be related to the shear stress as:

$$\frac{\Delta P}{2l} r = \tau \tag{1}$$

This paper assumes that the fluid's rheological behavior resembles the yielded power-law model. Consequently, we utilize the Herschel–Bulkley model (Hansong et al., 2004) [26].

$$\tau = \tau_y + k\dot{\gamma}^n \tag{2a}$$

Equating Equations (1) and (2a), we obtain:

$$\frac{\Delta P}{2l} r = \tau_y + k\dot{\gamma}^n \tag{2b}$$

where τ_y is the yield stress, k is the consistency index, and n is the flow index. The shear rate is the negative of the velocity gradient, $\dot{\gamma} = -\frac{du}{dr}$.

$$\int du = -\int \left(\frac{\Delta P}{2kl} r - \frac{\tau_y}{k} \right)^{1/n} dr \tag{3}$$

Integrating, we obtain:

$$u = -\frac{n}{(n+1)\frac{\Delta P}{2kl}}\left(\frac{\Delta P}{2kl}r - \frac{\tau_y}{k}\right)^{\frac{1}{n}+1} + C \tag{4}$$

The boundary condition stipulates that the fluid velocity at $r = r_p$ matches the pipe speed (V_p), while at the wellbore wall (i.e., $r = R_h$), the velocity equals zero. The integration constant, C, can be determined by applying the condition @$r = R_h$, $u = 0$, resulting in:

$$C = \frac{n}{(n+1)\frac{\Delta P}{2kl}}\left(\frac{\Delta P}{2kl}R_h - \frac{\tau_y}{k}\right)^{\frac{1}{n}+1} \tag{5}$$

By inserting the integration constant, the velocity of the disturbed fluid is expressed as:

$$u = \frac{n}{(n+1)\frac{\Delta P}{2kl}}\left(\frac{\Delta P}{2kl}R_h - \frac{\tau_y}{k}\right)^{\frac{1}{n}+1} - \frac{n}{(n+1)\frac{\Delta P}{2kl}}\left(\frac{\Delta P}{2kl}r_p - \frac{\tau_y}{k}\right)^{\frac{1}{n}+1} \tag{6}$$

Furthermore, by applying the second boundary condition, we assume that at $r = r_p$ (the outer diameter of the pipe), the fluid velocity along the pipe's wall is under the no-slip condition. It is important to note that this is to simplify the assumption.

$$V_p = \frac{n}{(n+1)\frac{\Delta P}{2kl}}\left(\frac{\Delta P}{2kl}R_h - \frac{\tau_y}{k}\right)^{\frac{1}{n}+1} - \frac{n}{(n+1)\frac{\Delta P}{2kl}}\left(\frac{\Delta P}{2kl}r_p - \frac{\tau_y}{k}\right)^{\frac{1}{n}+1} \tag{7}$$

Equation (7) represents a non-linear function. To facilitate the solution of the pressure gradient, we will temporarily assume $\frac{\tau_y}{k} = 0$ for the sake of simplicity. However, it is important to note that these effects will be reintroduced as a constant factor β later in our analysis.

$$V_p = \beta\left\{\frac{n}{(n+1)\frac{\Delta P}{2kl}}\left(\frac{\Delta P}{2kl}R_h\right)^{\frac{1}{n}+1} - \frac{n}{(n+1)\frac{\Delta P}{2kl}}\left(\frac{\Delta P}{2kl}r_p\right)^{\frac{1}{n}+1}\right\} \tag{8}$$

$$V_p = \frac{n\beta}{(n+1)}\left(\frac{\Delta P}{2kl}\right)^{\frac{1}{n}}\left\{(R_h)^{\frac{1}{n}+1} - (r_p)^{\frac{1}{n}+1}\right\} \tag{9}$$

Solving for the pressure gradient,

$$\frac{\Delta P}{l} = 2k\frac{\beta^{*n}(n+1)^n V_p^n}{n^n {R_h}^{n+1}\left\{1 - \left(\frac{r_p}{R_h}\right)^{\frac{1}{n}+1}\right\}^n} \tag{10}$$

whereas $\frac{r_p}{R_h}$ is the radius or diameter ratio $\frac{2r_p}{2R_h}$ and is replaced as $K = \frac{r_p}{R_h}$. The constant β^* replaced the constant $1/\beta$. The pressure gradient will be given as:

$$\frac{\Delta P}{l} = 2k\frac{\beta^{*n}\left(\frac{n+1}{n}\right)^n V_p^n}{{R_h}^{n+1}\left\{1 - K^{\frac{n+1}{n}}\right\}^n} \tag{11}$$

Experimental data has indicated that the pressure loss in an eccentric well geometry is typically less than 40% of that in a concentric well geometry. The pressure gradient in the eccentric well is determined by multiplying it by the reduction factor (R-factor) Haciislamoglu et al. (1990) [25]:

$$\left(\frac{\Delta P}{l}\right)_{Eccentric} = R\left(\frac{\Delta P}{l}\right)Concentric \tag{12}$$

.

Haciislamoglu et al. (1990) [25] conducted a series of experiments to account for the influence of eccentricity. They derived a correlation factor for the laminar flow of yield-power-law fluids within eccentric annuli. The authors compared their experimentally measured data with model predictions of pressure losses. These measurements were taken at various flow rates for two sets of rheological data. The dimensionless parameter, denoted as R, encapsulating the effect of eccentricity, is expressed as follows:

$$R = 1 - 0.072\frac{e}{n}\left(\frac{d_p}{d_h}\right)^{0.8454} - 1.5e^2\sqrt{n}\left(\frac{d_p}{d_h}\right)^{0.1852} + 0.96e^3\sqrt{n}\left(\frac{d_p}{d_h}\right)^{0.2527} \quad (13)$$

In the above equations, "e" represents the eccentricity of the drill string, "d_h" stands for the diameter of the wellbore, and "d_p" denotes the outer diameter of the inner pipe. Additionally, "(d_p/d_h)" corresponds to the ratio of the inner pipe diameter to the wellbore diameter.

It is important to note that the R-value has been generated based on the power-law fluid. However, this does not imply that the correlation will universally apply to all drilling fluid behaviors, such as the Herschel Bulkley and Bingham plastic models. This limitation arises because the model solely functions as a function of the flow index without accounting for other fluid rheological parameters, including yield stress, consistency index, and plastic viscosity. Nonetheless, in this paper, we used Haciislamoglu et al.'s (1990) [25] R-factor for the evaluation and modification.

In the modeling phase, we chose to exclude the $\frac{\tau_y}{k} = 0$ ratio due to the non-linearity of the equation, aiming to attain a simplified linearized model. However, apart from "k", we did not consider the influence of yield stress in this simplified model. To account for the impact of yield stress and "k'", we introduced the τ_y/k and "k/n" ratio for the yield-power-law and power-law models within Haciislamoglu et al.'s (1990) [25] Equation (13). These newly modified R-factors exhibit reasonable performance with the considered datasets, in conjunction with their associated β values, as indicated in the pressure loss gradient equation (Equation (11)). For yield-power-law fluid (Herschel–Bulkley), we obtained the new correlation factor R, which reads:

$$\begin{aligned} R_{YPL} = 1 - 0.08\frac{e}{n}\left(\frac{d_p}{d_h}\right)^{0.8454} - 1.5e^2\sqrt{n}\left(\frac{d_p}{d_h}\right)^{0.1852} + 0.96e^3\sqrt{n}\left(\frac{d_p}{d_h}\right)^{0.2527} \\ +0.045e^2\sqrt{n}\left(0.05\frac{\tau_y}{k}\right)^{2.875n}\left(\frac{d_p}{d_h}\right)^{0.5} \end{aligned} \quad (14)$$

In addition to the adjusted R_{YPL} factor, we determined a value for β^* in Equation (11) that effectively accommodates both yield-power-law and power-law fluids, and this value is found to be $\beta^* = 10$.

Regarding the power-law fluid, the newly introduced correlation factor can be expressed as:

$$\begin{aligned} R_{PL} = 1 - 0.072\frac{e}{n}\left(\frac{d_p}{d_h}\right)^{0.8454} - 1.5e^2\sqrt{n}\left(\frac{d_p}{d_h}\right)^{0.1852} + 0.96e^3\sqrt{n}\left(\frac{d_p}{d_h}\right)^{0.2527} \\ +0.045e^2\sqrt{n}\left(0.05\frac{k}{n}\right)^{2.875n}\left(\frac{d_p}{d_h}\right)^{0.5} \end{aligned} \quad (15)$$

Except for "k/n", all parameters are dimensionless. However, the constant 0.045 possesses the inverse unit, ensuring that the R-value remains dimensionless. Similarly, the value of β^* in Equation (11) is 15.5 for the power-law fluid.

3. Model Performance Analysis

In the subsequent sections, we will delve into the assessment of model performance, encompassing model testing and parameter sensitivity analysis. We evaluate the model's performance by computing the mean absolute average percentile deviation between the model predictions and the corresponding measured values to gauge the model's accuracy. Furthermore, we assess the variation of Srivastav et al.'s (2017) [12] model's predictions

from the measured values to ascertain the efficacy of the newly formulated model. In these evaluations, we employ the absolute mean error percentile, as introduced by Ochoa (2006) [27]:

$$Error_{ame} = \frac{1}{N}\sum_{i=1}^{N}\left|\frac{\left(\frac{\Delta P}{l}\right)_{measured} - \left(\frac{\Delta P}{l}\right)_{calculated}}{\left(\frac{\Delta P}{l}\right)_{measured}}\right| \times 100 \quad (16)$$

4. Model Testing

In the process of model evaluation, we have considered two power-law fluids (referred to as Fluid 1 and Fluid 2) as well as two yield-power-law fluids (referred to as Fluid 3 and Fluid 4). The rheological parameters for these fluids are detailed in Table 2. Notably, the power-law fluids have been composed of polyanionic cellulose (PAC) and, as a result, do not exhibit any yield stress characteristics. In contrast, the yield-power-law fluids have been formulated using xanthan gum and show noticeable yield stress.

Table 2. Fluid rheological parameters (Data, Srivastav et al. 2017 [12]).

Fluid	Rheology Model	Fluid Index n [ ]	Consistency Index k (lbf.s^n/100 ft^2)	Yield stress τ_y (lbf/100 ft^2)	Eccentricity (e)	d_h (in)	d_p (in)	d_p/d_h
Fluid 1	Power law	0.6343	2.78	0	0.9	2	1.32	0.66
Fluid 2		0.7363	0.83	0	0.9	2	1.32	0.66
Fluid 3	Yield Power Law	0.3255	6.4	20.9	0.9	2	1.32	0.66
Fluid 4		0.3428	2.52	6.20	0.9	2	1.32	0.66

4.1. Comparison of Pressure Loss Gradient Prediction of Power-Law Fluids

Srivastav et al. (2017) [12] conducted experiments to analyze the pressure loss gradient within a 0.9 eccentric annular geometry using power-law fluids while varying the string speed in the 0.1 to 0.8 ft/s range. We digitized both their model predictions and the experimental measurements for comparative purposes. Leveraging information regarding the drilling fluids and well geometry, we applied our new model (Equation (11)) in conjunction with the associated R-factors (R_{YPL}, as per Equation (14), and R_{PL}, as per Equation (15)) to compute the pressure loss gradient. Figures 2 and 3 present the results obtained for Fluids 1 and Fluid 2, respectively. Table 3 offers an analysis of the model's accuracy performance. Through visual inspection, it is evident that our new model's predictions closely align with the experimental measurements. Our model demonstrated the lowest mean discrepancy rate compared to Srivastav et al.'s (2017) [12] model's predictions.

4.2. Comparison of Pressure Loss Gradient Prediction of Yield-Power-Law Fluids

Likewise, the model predictions for the yield-power-law fluids (Fluids 3 and 4) are depicted in Figures 4 and 5, respectively. A summary of the model's performance analysis is presented in Table 4. These results again indicate that our model's predictions closely match a significant portion of the dataset compared with Srivastav et al.'s (2017) [12] model's predictions.

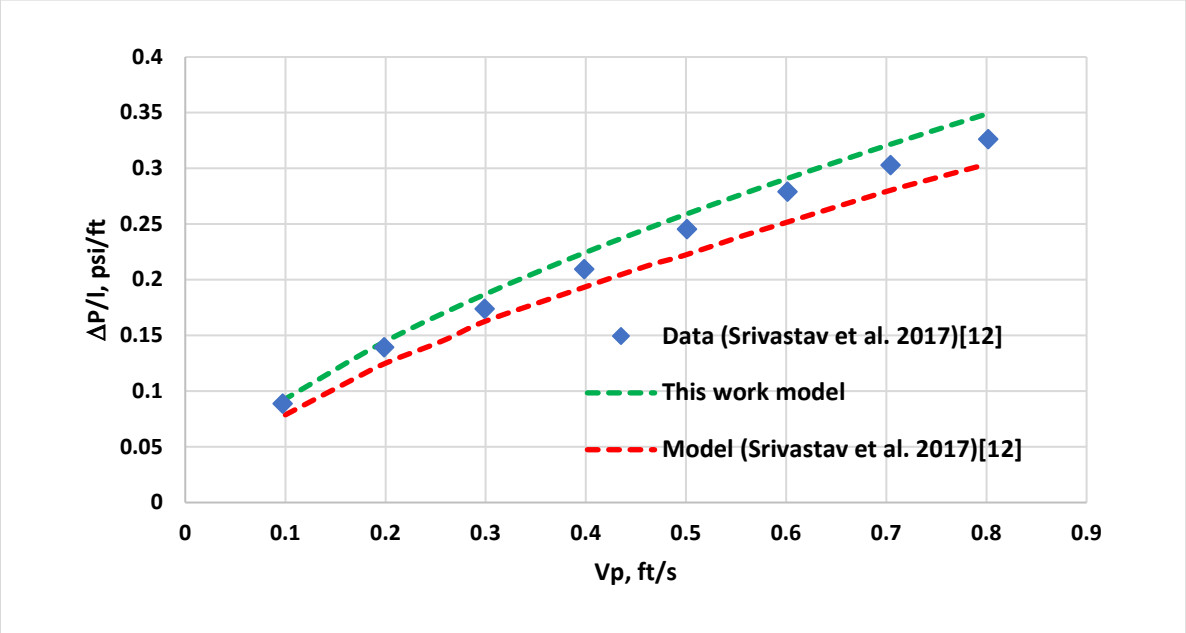

Figure 2. Pressure loss prediction with R_{PL} factor and measured power law—Fluid 1 [12].

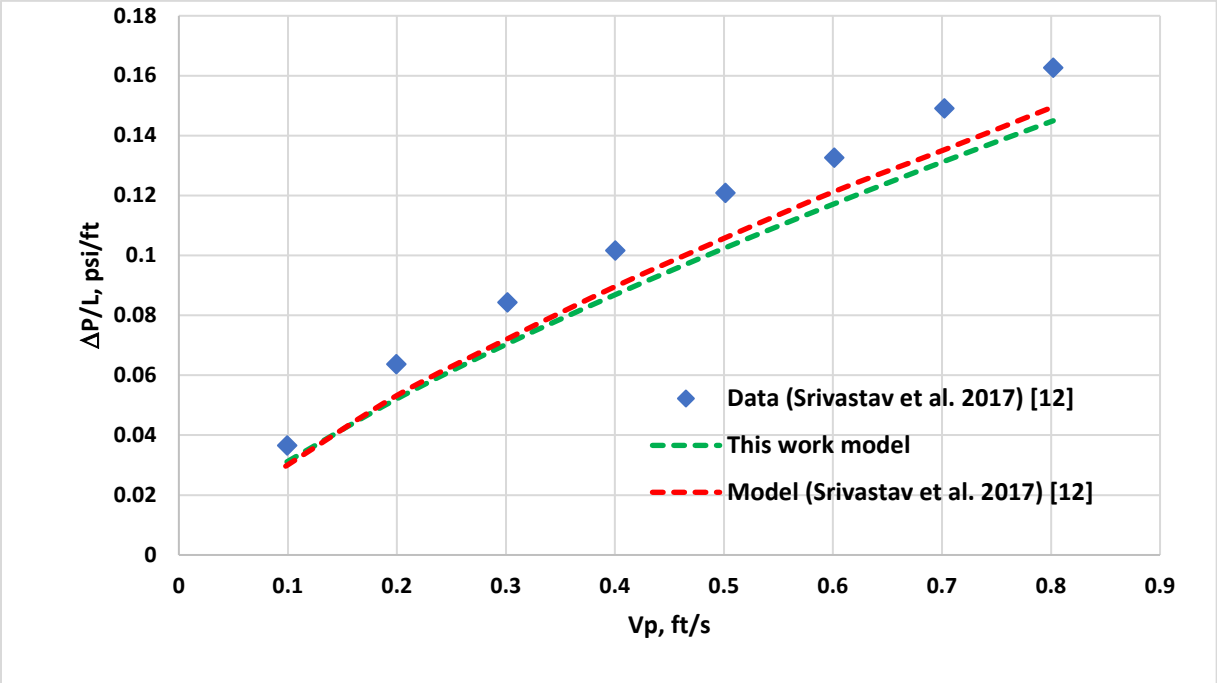

Figure 3. Pressure loss prediction with R_{PL} factor and measured power law—Fluid 2 [12].

Table 3. Model performance accuracy analysis for power-law fluids using this work R-factor.

Figure	Fluid	Model (This Work Equation (11))	Model (Srivastav et al., 2017) [12]	β^* This Model	This Work R-Factor
		Absolute Mean Error %			
Figure 2	Fluid 1	6.3	8.8	15.5	Equation (14)
Figure 3	Fluid 2	13.4	12.4	15.5	Equation (14)

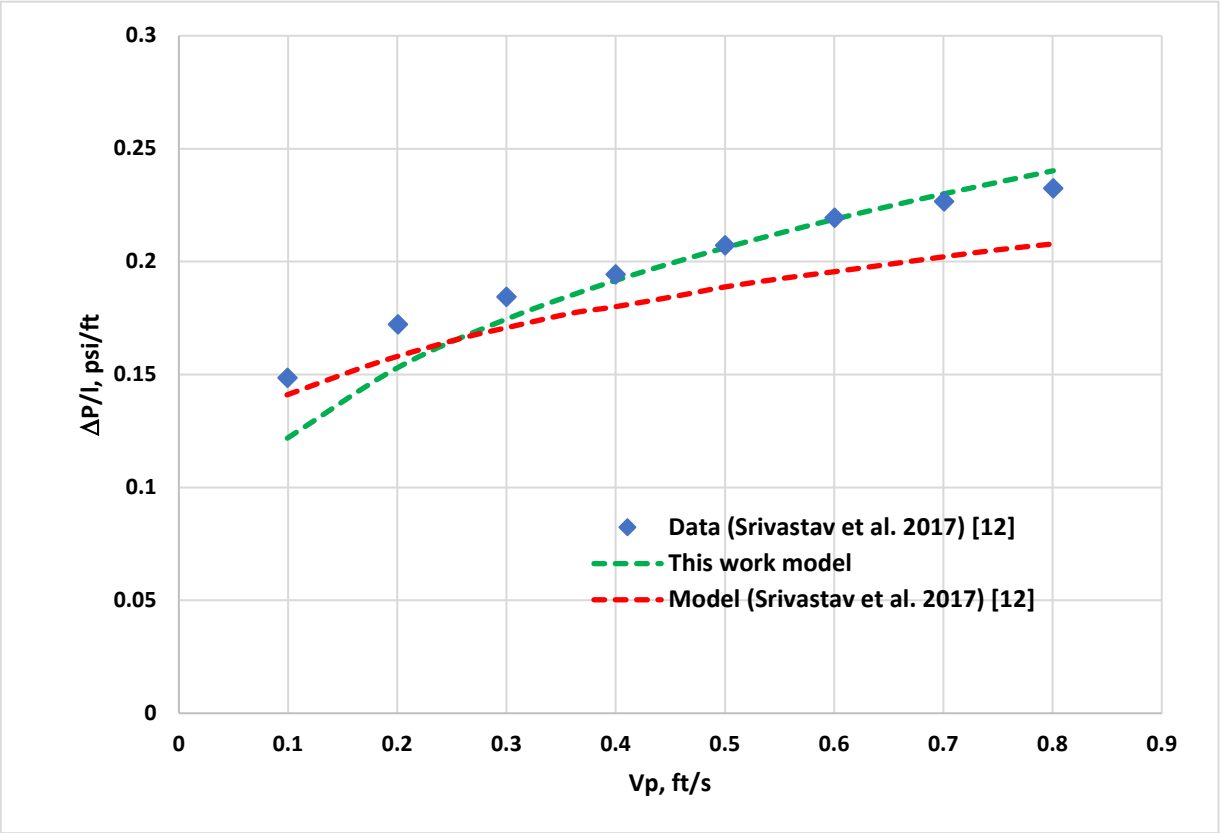

Figure 4. Pressure loss prediction with R_{YPL} factor and measured yield power law—Fluid 3 [12].

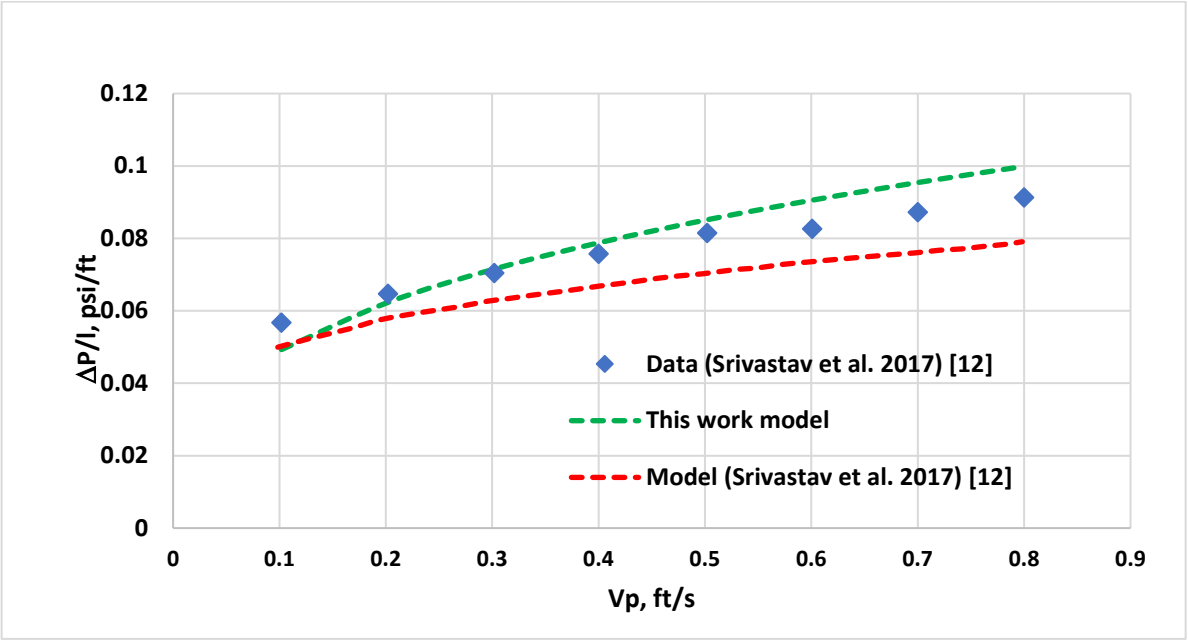

Figure 5. Pressure loss prediction with R_{YPL} factor and measured yield power law—Fluid 4 [12].

Table 4. Model performance accuracy analysis for the yield-power-law fluids using this work R-factor.

Figure	Fluid	Model (This Work Equation (11))	Model (Srivastav et al., 2017) [12]	β^* This Model	This Work R-Factor
		Absolute Mean Error %			
Figure 4	Fluid 3	5.2	8.7	10	Equation (15)
Figure 5	Fluid 4	6.9	11.7	10	Equation (15)

5. Parametric Sensitivity Analysis

Given the favorable performance demonstrated by the newly developed model, this section is dedicated to presenting numerical experiments that illustrate the influence of various parameters on the pressure gradient. The model is a function of several key variables, including tripping speed, pipe-to-well diameter ratio, consistency index, flow index, and yield strength of the drilling fluid. Therefore, to assess the impact of diameter ratio and eccentricity, the Srivastav et al.'s (2017) [12] power law and yield power-law fluids shown in Table 5 were considered. Moreover, to simulate the effect of flow index, dimeter ratio in eccentric geometry, fictitious fluids were assumed as shown in Table 6, To investigate the effect of the diameter ratio, we maintained the outer diameter (d_p) of the pipe at a constant value of 1.32 in. and varied the diameter of the well (d_h) as shown in the tables. The tripping speed has been set at a constant value of 0.5 ft/s, and two eccentric annuli (0.5 and 0.9) were used.

Table 5. Power law and modified power law fluids used to simulate the effect of diameter ratio in eccentric drill strings.

Fluid	Rheology Models	Rheological Parameters (Srivastav et al.'s (2017)) [12]			Drill Pipe/Well Geometry		
		n [ ]	k (lbf.s^n/100 ft^2)	τ_y (lbf/100 ft^2)	d_p (in)	d_h (in)	d_p/d_h
Fluid 1	Power Law	0.43	2.78	0	1.32	6.6	0.2
						3.3	0.4
Fluid 2		0.73	2.78	0		2.2	0.6
Fluid 3	Yield Power Law	0.3255	6.40	20.9		1.65	0.8
Fluid 4		0.3428	2.52	6.20		1.466	0.9

Table 6. Power law and modified power law fluids used to simulate the effect of flow index (n), diameter ratio and eccentricity.

Fluid	Rheology Models	Rheological Parameters			Drill Pipe/Well Geometry		
		n [ ]	k (lbf.s^n/100 ft^2)	τ_y (lbf/100 ft^2)	d_p (in)	d_h (in)	d_p/d_h
Fluid 5	Power Law	0.43	2.78	0	1.32	6.6	0.2
						3.3	0.4
Fluid 6		0.73	2.78	0		2.2	0.6
Fluid 7	Yield Power Law	0.43	2.78	6.20		1.65	0.8
Fluid 8		0.73	2.78	6.20		1.466	0.9

5.1. Dimeter Ratio and Eccentricity Effect on the Pressure Loss in Power-Law and Yield Power-Law Fluids

The drilling fluids and the well geometries used for the parametric sensitivity study are provided in Table 5. Figure 6 shows the simulated effect of diameter ratio on the pressure loss for the power-law fluids (1 and 2) filled in two eccentric wells. As the flow annular spacing reduces, the pressure loss increases. Since both fluids have the same consistency index, the difference in pressure loss is due to the flow index value. The impact is higher when the annulus is narrower. When the d_p/d_h is lower, the effect is insignificant.

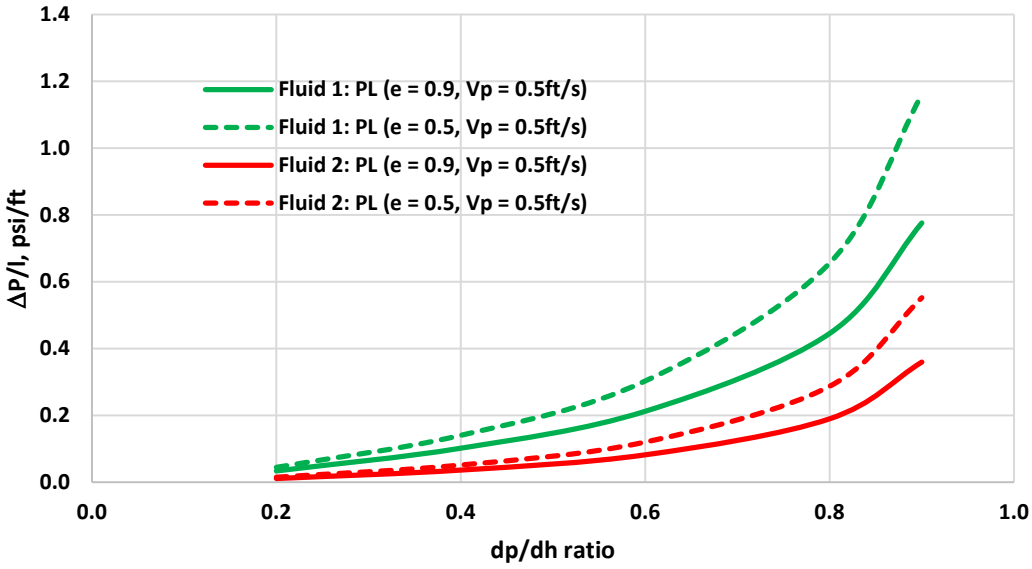

Figure 6. Effect of diameter ratio and eccentricity in power-law fluids.

Similarly, Figure 7 illustrates the impact of the pipe–well diameter ratio and eccentricity on the behavior of yield-power-law fluids.

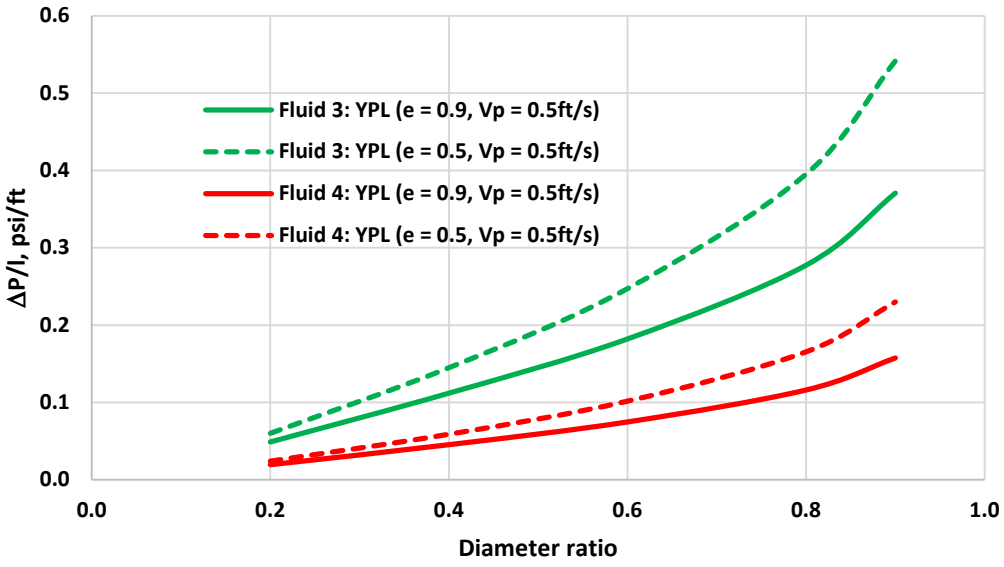

Figure 7. Effect of diameter ratio and eccentricity in the yield-power-law fluid.

5.2. Flow Index Effect on the Pressure Loss in Power-Law and Yield-Power-Law Fluids

The sensitivity analysis presented in Section 5.1 has revealed a pronounced impact of the pipe–well diameter ratio on the power law model, in contrast to its effect on yield-power-law (YPL) fluids. To further evaluate the model's reliability, we have devised a series of new experiments to investigate the model's sensitivity to changes in the fluid index "*n*" value of the fluids. In these experiments, the consistency index of both fluids remains constant, while the fluid index "*n*" values are systematically adjusted to 0.43 and 0.73. Notably, the yield strengths of the yield-power-law fluids remain constant throughout these experiments. The fluid properties are provided in Table 6.

The simulation was conducted with an eccentricity of 0.9 and a tripping speed of 0.5 ft/s. Figure 8 presents the results of this simulation. It is evident that for n = 0.73, both power-law (PL) and yield-power-law (YPL) fluids exhibited a higher pressure loss, with the effect being more pronounced in the power law model than in the yield power law

model. Notably, the R-value of the power law effect remains consistent with the R-factor established by Haciislamoglu et al. (1990) [25]. This outcome is primarily attributed to the fact that the coefficient of the first term was left unaltered, and the influence of the last term on the behavior of the considered fluids was not significant.

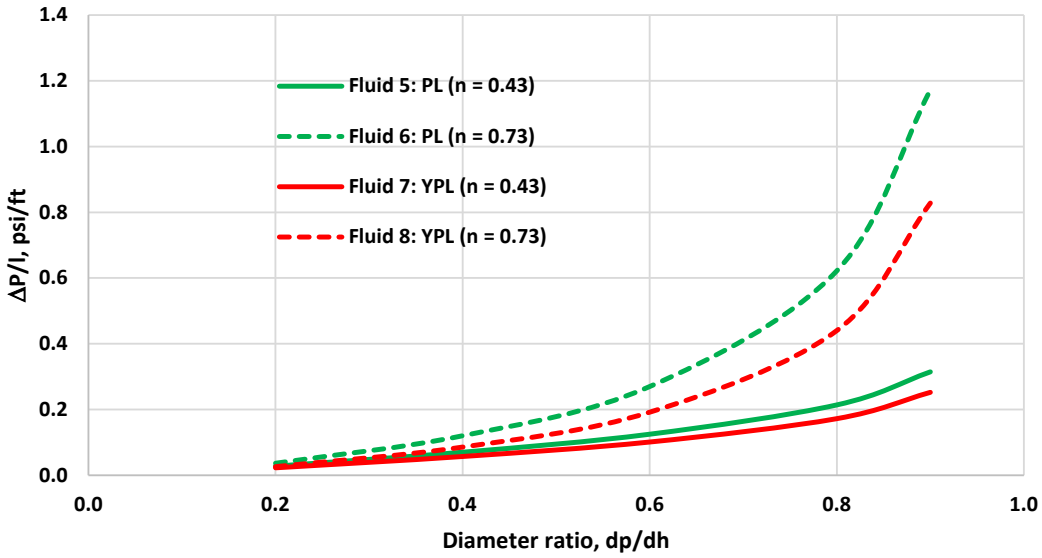

Figure 8. Effect of flow index (*n*) on the PL and YPL fluids' pressure loss vs. diameter ratio.

In contrast, for the yield power law model, adjustments were made to the first terms, transitioning from 0.072 to 0.08, while the effect of the last included term on the behavior of the considered fluids remained inconsequential. As Figure 9 illustrates, the behavior of the yield power law deviates from that found by Haciislamoglu et al. [25] and the power law R-value, particularly for higher diameter ratios. However, this discrepancy is not exceedingly pronounced. The elevated pressure observed in both the power law and yield power law models can be attributed to the β^* values derived from the experimental dataset. Additional comparative assessments are required to validate the model further.

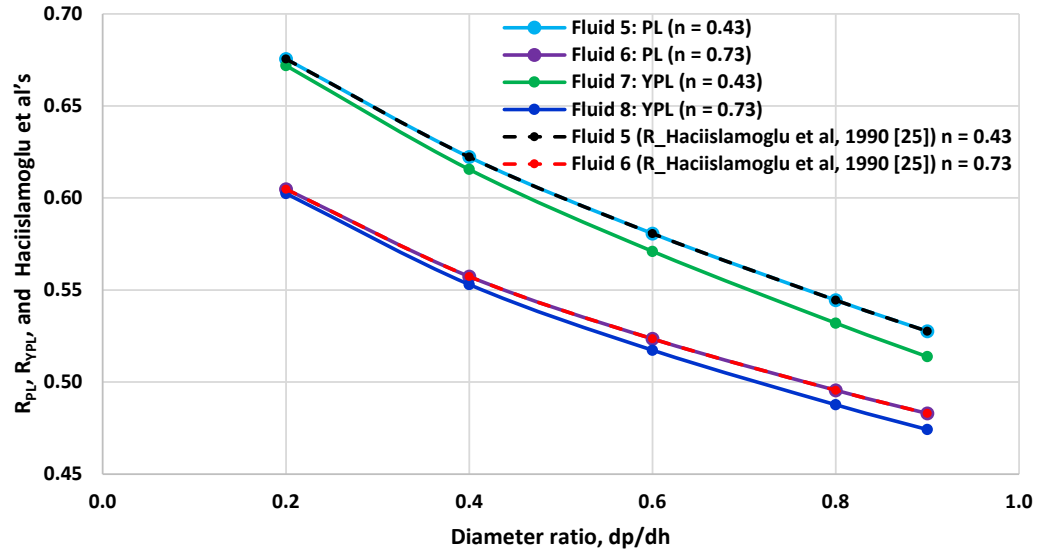

Figure 9. Effect of flow index (*n*) on the R-factors (R_{PL} (Equation (15)), R_{YPL} (Equation (14)), Haciislamoglu et al. (1990) [25] (Equation (13))) vs. diameter ratio for e = 0.9 and k = 2.75 lbf-s^n/100 ft^2.

6. Determination of Power and Yield Power Law β* Constant for Haciislamoglu et al.'s R-Factor

In the following section, we aim to couple the power-law and yield-power-law fluids parameters to the R-factor proposed by Haciislamoglu et al. (1990) [25]. The sensitivity study results shown in Figure 9 indicate that the R-value variation is 0.01 when the diameter ratio is higher. In this subsequent section, we aim to determine the beta factors when both fluids have the R-factor, as Haciislamoglu et al. [25]. The analysis results show the optimized beta factor for power-law fluids with $\beta^* = 15.8$ and yield-power-law fluids with $\beta^* = 9.5$. Figures 10–13 show the model predictions and the measured datasets. Table 7 shows the summary of the model's performance accuracy analysis. For the power-law Fluid 1, the new beta factors reduced the error but produced nearly equal performance to Srivastav et al.'s [12] model for Fluid 2. On the other hand, the new beta factors performance for fluids 3 and 4 are better than the Srivastav et al.'s (2017) [12] model's prediction.

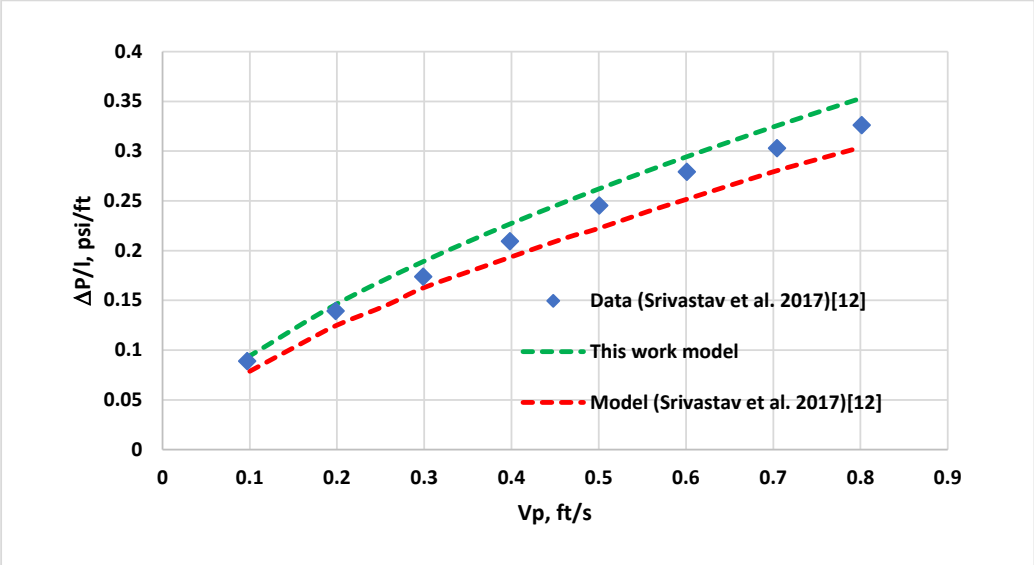

Figure 10. Pressure loss prediction with Haciislamoglu et al.'s [25] R-factor and measured power law—Fluid 1 [12].

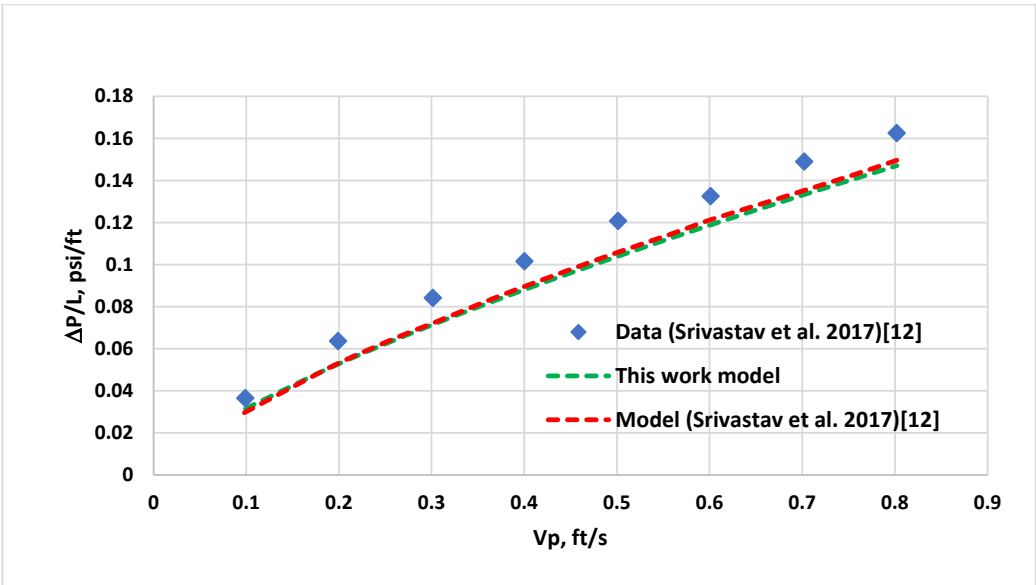

Figure 11. Pressure loss prediction with Haciislamoglu et al.'s [25] R-factor and measured power law—Fluid 2 [12].

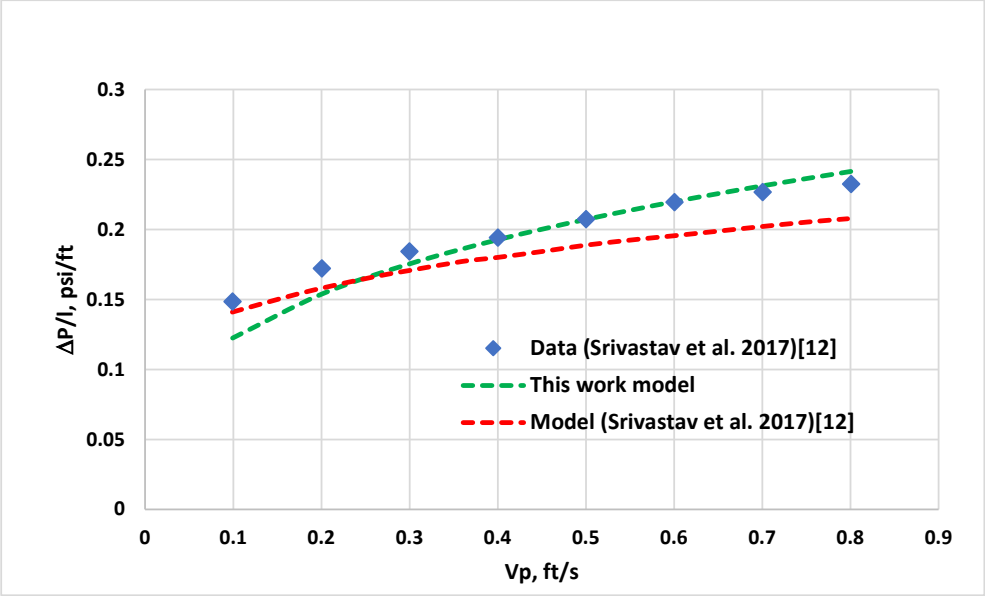

Figure 12. Pressure loss prediction with Haciislamoglu et al.'s [25] R-factor and measured yield power law—Fluid 3 [12].

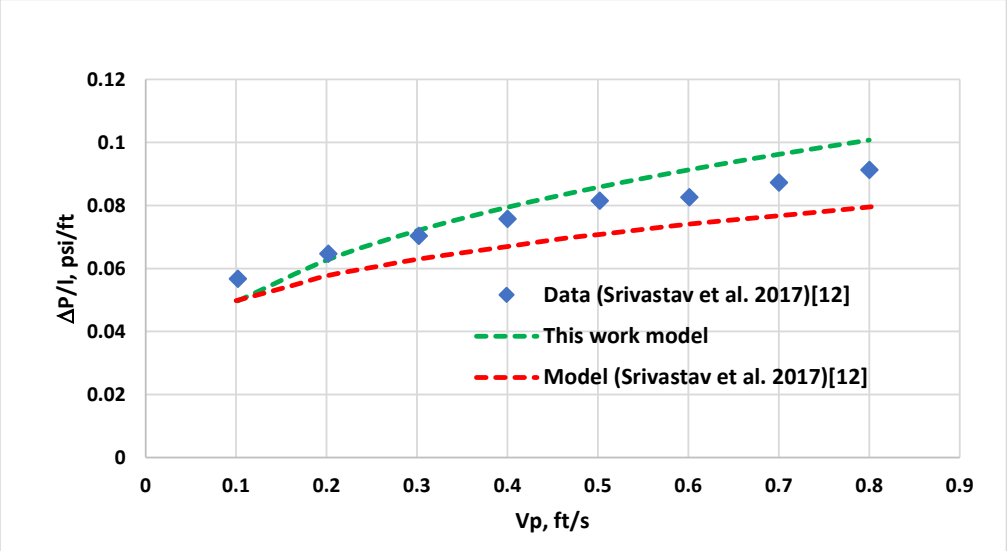

Figure 13. Pressure loss prediction with Haciislamoglu et al.'s [25] R-factor and measured yield power law—Fluid 4 [12].

Table 7. Model performance accuracy analysis for the power and yield-power-law fluids using Haciislamoglu et al.'s [25] R-factor.

Figure	Fluid	Model (This Work Equation (11))	Model (Srivastav et al., 2017) [12]	β^* This Model	R-Factor [25]
		Absolute Mean Error %			
Figure 10	Fluid 1	6.8	8.8	15.8	Equation (13)
Figure 11	Fluid 2	13.0	12.4	15.8	Equation (13)
Figure 12	Fluid 3	5.0	8.7	9.5	Equation (13)
Figure 13	Fluid 4	7.4	11.7	9.5	Equation (13)

7. Discussion

During tripping operation, the axial movement of pipes generates fluid disturbance; hence, differential pressure develops. In this study, we developed a simple analytical hydraulics model that predicts the pressure gradient as pipe moves axially in the power-law and yield-power-law fluids. The model assumes that the fluid is incompressible and under steady-state conditions. The model performance accuracy analysis has been conducted by comparing the model prediction with the swab/surge experimental test data measured in 0.9 eccentric annuli filled with two power-law and two yield-power-law fluids by Srivastav et.al. (2017) [12].

In Section 3, due to the non-linear nature of the newly derived model, we simplify the problem by momentarily neglecting the yield stress and consistency index. In this way, a linear model was obtained. To take into account the effect of the omitted stress/viscosity ratio (Equation (7)), two modifications were included in the linear model and the R-factor of Haciislamoglu et al. (1990) [25]. The reason for the modification in the R-factor is that Haciislamoglu et al.'s (1990) [24] R-factor is a function of power-based parameters only.

In Section 4, we compared the model's effectiveness using Srivastav et al.'s (2017) [12] experimental dataset. Moreover, the model prediction was also analyzed by comparing it to Srivastav et al.'s (2017) [12] model. The first part of the model performance evaluation was conducted by using the R_{PL} (Equation (14)) and R_{YPL} (Equation (15)) modified R-factors (Equation (13)), which are used for the power-law fluids and the yield-power-law fluids, respectively. For these R factors, the optimized β^* values have been obtained. The surprising result was that both power-law fluids showed β^* values of 15.5, and the yield-power-law fluid showed a β^* value of 10. The mean absolute sum between the model prediction and the measurement values computed results showed that the newly developed model's performance is relatively better than Srivastav et al.'s (2017) [12] model.

The beta factor (β^*) for the power-law fluid is higher than that of the yield-power-law fluid when using the modified R-factors (Equations (14) and (15)). However, in Section 6, using Haciislamoglu et al.'s (1990) [25] R-factor, the magnitudes of the beta factor of the two fluids were analyzed. Results show that the best-fit model prediction for the power-law and the yield-power-law fluids were obtained when beta values were $\beta^* = 15.8$ and $\beta^* = 9.5$, respectively. The model performance analysis also shows that the new model prediction reduced the error between the model and the measurement results from Sections 4 and 6, indicating that both modeling results are fairly similar and show improved performances.

Moreover, in Section 5, fictitious fluids have been formulated (Fluids 5–8) by varying the flow index and yield stress values while keeping the consistency index constant. The attempt was to investigate the impact of flow index in the assumed power and yield-power fluids. Results showed that the pressure loss gradient increased as the curvature exponent rose from 0.43 to 0.73. The lower "n" value showed higher R-factors. However, the "n" value in the pressure was dominant for the higher R-factor. One can also observe that the impact of "n" on the power-law fluid showed a higher R-factor than the yield-power-law fluid by 0.01 when the diameter ratio is about 0.9. The difference is insignificant for the lower diameter ratio. On the other hand, the power-law-based modified R-factor results are almost the same as the Haciislamoglu et al. (1990) [25] R-factor results.

The model comparison and sensitivity study analysis performed well, and the trends are as expected. However, the model performance evaluation should be further assessed with other literature and field datasets. The model is limited to the impact of drill string axial speed and the fluid flow effect. As a future work, the fluid flow velocity would be coupled with the tripping rate and tested with the available literature-based dataset. Moreover, since the model is linearized and model calibration, the beta factor has been introduced, making solving the non-linear model (Equation (11)) with a numerical method possible. However, models require a calibration factor, which should be determined from measured data. This paper aimed to investigate the impact of parameters and study the pressure loss model prediction of power-law and yield-power-law fluids.

As indicated in Table 7, the model predictions have been applied to both power-law and yield-power-law model fluids. These predictions were also compared with the model proposed by Srivastav et al. (2017) [12]. The average percentile error deviation between our model and the measured data was calculated. Our model (Equation (11)) shows error deviations of 9.9% and 6.2% for power-law and yield-power-law fluids, respectively. In contrast, Srivastav et al.'s (2017) [12] model records 10.6% and 10.2%, respectively.

It is crucial to note that these results are valid for the considered fluid systems. However, variations in fluid systems, operations, and geometrical conditions may impact the model's performance differently. For instance, Jeyhun et al. (2016) [28] assessed the predictive capabilities of six hydraulic models using field- and laboratory-measured data. The analysis revealed that while one hydraulic model predicted perfectly for Fluid Type A, a different model worked better for Fluid Type B. This study emphasized that the model's prediction could vary with changes in fluid rheological parameters.

The swab and surge simulation studies carried out by Amir et al. (2023) [23] revealed that the hydraulic predictions of the three considered models (Bingham plastic, power law, and Robertson and Stiff) were inconsistent across various well trajectories and fluid rheological types.

Considering this observation, the results presented in this paper indicate the need for further model testing to ascertain the limits of the model's applicability.

8. Conclusions

We have developed a simplified analytical model for swabs and surges in this study. This model considers eccentricity, diameter ratio, fluid rheological properties, and tripping speed. We conducted experiments using two power-law and two yield-power-law fluids formulated with PAC- and xanthan-gum-based polymers to validate the model. Our findings can be summarized as follows:

- The model has shown good prediction of the experimental data when utilizing specific β^* values and R-factors for power-law and yield-power-law fluids.
- The rheological properties of fluids, diameter ratio, and tripping speed influence pressure variations during swabs and surges.
- The modified R-factor presented in this paper suggests that it could be further adapted for different fluid properties.
- The β^* value for yield-power-law fluids is lower compared to power-law fluids, resulting in lower pressure loss in yield-power-law fluids.
- Increasing the "n" value increases pressure losses in both power-law and yield-power-law fluids.
- Similarly, an increase in the "k" value results in higher pressure losses in both power-law and yield-power-law fluids.
- The overall model comparison results showed average percentile error deviations of 9.9% and 6.2% for the power-law and yield-power-law fluids, respectively.

Finally, this paper demonstrates that physics-based models are adequate for the given type of drilling fluid, highlighting the suitability of a rheology model to describe the drilling fluid. It does mean that the hydraulics model predicts the pressure loss for that particular fluid type. It is, therefore, always important to have measurements and do model calibration. In the calibration factors, hidden physical parameters exist that the model did not consider. In this regard, applying a machine learning model that utilizes a measured dataset includes all the factors affecting the measurement. Hence, machine learning models have shown promising results in many fields.

Author Contributions: A.M.: conceptualization, methodology, testing, sensitivity analysis, model performance analysis, interpretation, and writing. M.B.: methodology, draft manuscript preparation, supervision, review, and editing. All authors have read and agreed to the published version of the manuscript.

Funding: This research received no external funding.

Institutional Review Board Statement: Not applicable.

Informed Consent Statement: Not applicable.

Data Availability Statement: The data presented in this study are openly available in [12].

Conflicts of Interest: The authors declare no conflict of interest.

Nomenclature

d_h	Hole diameter (in)
d_p	Pipe diameter (in)
$K = d_p/d_h$	Pipe to hole diameter ratio
e	Eccentricity
l	Length (ft)
k	Consistency index (lbf.s^n/100 ft^2)
n	Flow index
r_p	The outer radius of the pipe (in)
R	R-factor
R_h	Inner radius of the wellbore (in)
$R_{\_YPL}$	R-factor for yield power law
$R_{\_PL}$	R-factor for power law
u	Velocity of fluid (ft/s)
V_p	Pipe tripping speed (ft/s)
β^*	Constant
β	Constant
$\dot{\gamma}$	Shear rate (1/s)
τ	Shear stress (lbf/100 ft^2)
τ_y	Yield stress (lbf/100 ft^2)
$\Delta P/l$	Differential pressure per length (psi/ft)

References

1. Hovda, S.; Wolter, H.; Kaasa, G.O.; Ølberg, T.S. Potential of Ultra High—Speed Drill String Telemetry in Future Improvements of the Drilling Process Control. In Proceedings of the IADC/SPE Asia Pacific Drilling Technology Conference and Exhibition, Jakarta, Indonesia, 25–27 August 2008.
2. Rehm, B.; Schubert, J.; Haghshenas, A.; Hughes, J.; Paknejad, A.S. *Managed Pressure Drilling*; Elsevier: Amsterdam, The Netherlands, 2013.
3. Pilisi, N.; Wei, Y.; Holditch, S.A. Selecting Drilling Technologies and Methods for Tight Gas 476 Sand Reservoirs. In Proceedings of the 2010 IADC/SPE Drilling Conference, New Orleans, LA, USA, 2–4 February 2010.
4. Redden, J. Advanced Fluid Systems Aim to Stabilize Well Bores, Minimize Nonproductive Time. *American. Oil Gas Rep.* **2009**, *52*, 58–65.
5. Halland, T.; Meisal, K.I.; Abramsen, T.; Morrison, P. New data transfer protocol improves drilling support and safety. In *World Oil*; Gulf Publishing Company: Houston, TX, USA, 2018; pp. 39–42.
6. Burkhardt, J.A. Wellbore pressure surges produced by pipe movement. *J. Pet. Technol.* **1961**, *13*, 595–605. [CrossRef]
7. Schuh, F.J. Computer makes surge-pressure calculations useful. *Oil Gas J.* **1964**, *31*, 96.
8. Fontenot, J.E.; Clark, R.K. An improved method for calculating swab and surge pressures and circulating pressures in a drilling well. *Soc. Pet. Eng. J.* **1974**, *14*, 451–462. [CrossRef]
9. Mitchell, R.F. Dynamic surge/swab pressure predictions. *SPE Drill. Eng.* **1988**, *3*, 325–333. [CrossRef]
10. Ahmed, R.; Miska, S. Experimental study and modeling of yield power-law fluid flow in annuli with drillpipe rotation. In Proceedings of the SPE/IADC Drilling Conference and Exhibition, Orlando, FL, USA, 4–6 March 2008.
11. Crespo, F.; Ahmed, R.; Saasen, A. Surge and swab pressure predictions for yield-power-law drilling fluids. In Proceedings of the SPE Latin American & Caribbean Petroleum Engineering Conference, Lima, Peru, 1–3 December 2010.
12. Srivastav, R.; Ahmed, R.; Saasen, A. Experimental Study and Modeling of Surge and Swab Pressures in Horizontal and Inclined Wells. In Proceedings of the AADE-17-NTCE-075 Technical Conference and Exhibition, Houston, TX, USA, 11–12 April 2017.
13. Gjerstad, K.; Time, R.W.; Bjorkevoll, K.S. A Medium-Order Flow Model for Dynamic Pressure Surges in Tripping Operations; In Proceedings of the SPE/IADC Drilling Conference, Amsterdam, The Netherlands, 5–7 March 2013.
14. Tang, M.; Ahmed, R.; Srivastav, R.; He, S. Simplified surge pressure model for yield power law fluid in eccentric annuli. *J. Pet. Sci. Eng.* **2016**, *145*, 346–356. [CrossRef]
15. Crespo, F.; Ahmed, R.; Enfis, M.; Saasen, A.; Amani, M. Surge-and-Swab Pressure Predictions for Yield-Power-Law Drilling Fluids. *SPE Drill. Complet.* **2012**, *27*, 574–585. [CrossRef]

16. Erge, O.; Ozbayoglu, E.M.; Miska, S.Z.; Yu, M.; Takach, N.; Saasen, A.; May, R. The Effects of Drillstring-Eccentricity, -Rotation, and -Buckling Configurations on Annular Frictional Pressure Losses While Circulating Yield-Power-Law Fluids. *SPE Drill. Complet.* **2015**, *30*, 257–271. [CrossRef]
17. He, S.; Tang, M.; Xiong, J.; Wang, W. A numerical model to predict surge and swab pressures for yield power law fluid in concentric annuli with open-ended pipe. *J. Pet. Sci. Eng.* **2016**, *145*, 464–472. [CrossRef]
18. Ozbayoglu, E.M.; Erge, O.; Ozbayoglu, M.A. Predicting the pressure losses while the drill string is buckled and rotating using artificial intelligence methods. *J. Nat. Gas Sci. Eng.* **2018**, *56*, 72–80. [CrossRef]
19. Ettehadi, A.; Altun, G. Functional and practical analytical pressure surges model through Herschel Bulkley fluids. *J. Pet. Sci. Eng.* **2018**, *171*, 748–759. [CrossRef]
20. Krishna, S.; Ridha, S.; Vasant, P. Prediction of Bottom-Hole Pressure Differential during Tripping Operations Using Artificial Neural Networks (ANN). In *Intelligent Computing and Innovation on Data Science*; Springer: Singapore, 2020; Volume 118, pp. 379–388.
21. Belimane, Z.; Hadjadj, A.; Ferroudji, H.; Rahman, M.A.; Qureshi, M.F. Modeling surge pressures during tripping operations in eccentric annuli. *J. Nat. Gas Sci. Eng.* **2021**, *96*, 104233. [CrossRef]
22. Mohammad, A.; Karunakaran, S.; Panchalingam, M.; Davidrajuh, R. Prediction of Downhole Pressure while Tripping. In Proceedings of the 2022 14th International Conference on Computational Intelligence and Communication Networks (CICN), Al-Khobar, Saudi Arabia, 4–6 December 2022; pp. 505–512.
23. Mohammad, A.; Belayneh, M.; Davidrajuh, R. Physics-Based Swab and Surge Simulations and the Machine Learning Modeling of Field Telemetry Swab Datasets. *Appl. Sci.* **2023**, *13*, 10252. [CrossRef]
24. Krishna, S.; Ridha, S.; Vasant, P.; Ilyas, S.U. New analytical approach for predicting surge/swab pressure gradient using mud clinging effect and frictional pressure losses: For yield power-law fluid. In Proceedings of the Offshore Technology Conference Asia, Kuala Lumpur, Malaysia, 2–6 November 2020.
25. Haciislamoglu, M.; Langlinais, J. Non-Newtonian flow in eccentric annuli. *J. Energy Resour. Technol.* **1990**, *112*, 163–169. [CrossRef]
26. Tang, H.S.; Kalyon, D.M. Estimation of the parameters of Herschel-Bulkley fluid under wall slip using a combination of capillary and squeeze flow viscometers. *Rheol. Acta* **2004**, *43*, 80–88. [CrossRef]
27. Ochoa, M.V. *Analysis of Drilling Fluid Rheology and Tool Joint Effect to Reduce Errors in Hydraulics Calculations*; Texas A&M University: College Station, TX, USA, 2006.
28. Sadigov, J.; Belayneh, M. Analyses of Field Measured Data with Rheology and Hydraulics Models. *Int. J. Fluids Eng.* **2016**, *8*, 1–12.